



High-quality Cu₂ZnSnS₄ and Cu₂ZnSnSe₄ nanocrystals hybrid with ZnO and NaYF₄: Yb, Tm as efficient photocatalytic sensitizers

Yawei Yang^a, Wenviu Que^{a,*}, Xinyu Zhang^b, Xingtian Yin^a, Yonglei Xing^a, Meidan Que^a, Hongyang Zhao^b, Yaping Du^{b,*}

^a Electronic Materials Research Laboratory, International Center for Dielectric Research, Key Laboratory of the Ministry of Education, School of Electronic & Information Engineering, Xi'an Jiaotong University, Xi'an 710049, Shaanxi, PR China

^b Frontier Institute of Science and Technology jointly with College of Science, State Key Laboratory for Mechanical Behavior of Materials, Xi'an Jiaotong University, Xi'an 710049, Shaanxi, PR China

ARTICLE INFO

Article history:

Received 10 May 2016

Received in revised form 29 June 2016

Accepted 16 July 2016

Available online 18 July 2016

Keywords:

Cu₂ZnSnS₄

Cu₂ZnSnSe₄

Hydrophilic treatment

Rare earth upconversion

Photocatalytic sensitizer

ABSTRACT

A chloroform-assistant Se dissolution in oleylamine without trioctylphosphine and alkylthiol as the green precursor was used for facile and robust synthesis of quaternary selenide nanocrystals. The S²⁻ modified hydrophilic Cu₂ZnSnS₄ and Cu₂ZnSnSe₄ nanocrystals were first prepared by a one-pot thermal decomposition route, followed by a bi-phase hydrophilic treatment process. As a proof of concept, the as-obtained hydrophilic nanocrystals were hybridized with ZnO microspheres as photosensitizers to achieve visible light-driven photocatalytic application; on the other hand, hybridized with NaYF₄: Yb, Tm microplates to achieve near-infrared light-driven photocatalytic application. These photosensitized hybrids as photocatalysts expanded the light absorption from ultraviolet to visible even near-infrared region, which showed excellent photocatalytic Rhodamine B degradation under visible and near-infrared irradiation compared to pure ZnO and NaYF₄: Yb, Tm, respectively. Therefore, these hydrophilic Cu₂ZnSnS₄ and Cu₂ZnSnSe₄ nanocrystals are proved as efficient photocatalytic sensitizers due to the efficient utilization of the visible light and emissions upconverted from near-infrared light.

© 2016 Elsevier B.V. All rights reserved.

1. Introduction

Organic pollution in water has been one of the most serious environmental problems over the last decade, and semiconductor photocatalytic degradation by employing solar energy has been considered as an economic and safe solution to this issue [1]. However, one challenge for photocatalysis is the typical semiconductors (e.g. TiO₂ and ZnO) have narrow absorption range of the sunlight [only ultraviolet (UV) light] [2]. Utilization of solar energy in visible (Vis) and near-infrared (NIR) regions, which comprise ~50% and ~45% of the solar spectrum, respectively, is still an arduous task for photocatalysis. To overcome these limitations, photosensitization with narrow bandgap semiconductors have been developed to achieve Vis light response for wide bandgap materials [3], and combination with rare earth upconversion materials [typically NaYF₄: Yb, Tm (NYF)] as light converters have been proposed to achieve NIR light response [4]. NYF/TiO₂ composites have been reported as promising NIR light-driven photocatalysts [5–9]. More-

over, combination of upconversion materials with narrow bandgap semiconductors would be a better candidate to improve the utilization of all the upconverted emissions, especially Vis ones [10,11].

Although several binary, ternary and quaternary chalcogenide semiconductor sensitizers have been studied intensively for sunlight harvest [12–18], Cu₂ZnSnS₄ (CZTS) and Cu₂ZnSnSe₄ (CZTSe) uniquely combine both superior optoelectronic properties with high absorption coefficient over 10⁴ cm⁻¹, strong stability and suitable direct bandgap energy (1.0–1.5 eV) [19–21]; and chemical compositions based on earth-abundant elements. Such low-cost and environment-friendly quaternary compounds have been attracted intensive interest in the field of photovoltaic conversion [22], thermoelectric conversion [23], photocatalytic pollutant degradation [24], water splitting [25] and CO₂ reduction [26]. Recently, various methods have been developed to prepare this kind of quaternary light absorbers [24,27–34]. Among these methods, one-pot thermal decomposition method provides the facile controllability and large scale possibility for CZTS(e) nanocrystals preparation [35]. To our best knowledge, Se powder has poor solubility in common solvents [typically oleylamine (OLA)]. This problem has been solved by (1) using the alternative highly reactive organic selenium precursors [36,37]; (2) dissolving Se powder in trioctylphosphine (TOP) or trioctylphosphine oxide (TOPO) [38];

* Corresponding authors.

E-mail addresses: wxque@mail.xjtu.edu.cn (W. Que), ypdu2013@mail.xjtu.edu.cn, ypdupku@gmail.com (Y. Du).

(3) reducing Se powder with NaBH_4 [39] or alkylthiol [40] in the presence of OLA; and (4) dissolving Se or SeO_2 in 1-octadecene (ODE) at 180 °C under inert atmosphere [35,41]. The issues of expensive, toxic, unstable, S doping, and complex operation are still remained, respectively. Here, we have developed a green TOP and alkylthiol-free Se precursor by dissolving Se powder in oleylamine with the help of chloroform under ambient condition, which explores as a viable alternative for the synthesis of high-quality selenide nanocrystals.

Nanocrystals obtained from thermal decomposition in OLA have small and uniform in size distribution, which have strong nanosize effect and beneficial for photocatalysis. However, the nanocrystals with hydrophobic ligands on their surfaces hinder their dispersion in aqueous solution and charge transfer between adjacent nanocrystals. Therefore, the surface modification is required to overcome these problems in practical applications. Up to now, many kinds of capping ligands have been successfully applied to achieve highly hydrophilic state and electronic transportation [42–46]. Among these ligands, the nontoxic inorganic S^{2-} coordinated with the nanocrystals, provide electrostatic stabilization in polar solvents without affecting their nanosize effect [45].

To our best knowledge, there are few reports on the CZTS(e) nanocrystals as sensitizers in photocatalytic application. Herein, we demonstrated a facile and robust process for preparing S^{2-} modified hydrophilic CZTS(e) nanocrystals. High-quality monodisperse nanocrystals were prepared by a one-pot thermal decomposition route. The hydrophilic nanocrystals were further obtained through a bi-phase hydrophilic treatment process. Then the hydrophilic nanocrystals were hybridized with ZnO microspheres and NYF microplates as photosensitizers in Vis and NIR light-driven photocatalytic reactions, respectively (Scheme 1). The $\text{ZnO}/\text{CZTS}(e)$ and $\text{NYF}/\text{CZTS}(e)$ hybrids showed excellent photocatalytic Rhodamine B (RhB) degradation under Vis and NIR irradiation compared to pure ZnO and NYF, respectively, proving the efficient utilization of the Vis light and emissions upconverted from NIR light of the CZTS(e) nanocrystals.

2. Experimental

2.1. Materials

$\text{Cu}(\text{OAc})_2 \cdot \text{H}_2\text{O}$ (98.0%), $\text{Zn}(\text{OAc})_2 \cdot 2\text{H}_2\text{O}$ (99.0%), $\text{SnCl}_2 \cdot 2\text{H}_2\text{O}$ (98.0%), trisodium citrate (99.0%), NaF (98.0%), N,N -dimethyl formamide (DMF, 99.5%), diethylene glycol (99.0%), chloroform (99.0%), cyclohexane (99.5%) and ethanol (99.7%) were purchased from Sinopharm. S (99.5%) and Se (99.5%) were purchased from Alfa-Aesar. $\text{Na}_2\text{S} \cdot 9\text{H}_2\text{O}$ (99.99%) were purchased from Aladdin. $\text{YCl}_3 \cdot 6\text{H}_2\text{O}$ (99.99%), $\text{YbCl}_3 \cdot 6\text{H}_2\text{O}$ (99.99%), and $\text{TmCl}_3 \cdot 6\text{H}_2\text{O}$ (99.99%) were purchased from Energy Chemical. Oleylamine (OLA, 70%) were purchased from Aldrich. All chemicals used in this work were used as received without further purification. Ultrapure water was used throughout the experiments.

2.2. Synthesis of CZTS(e) nanocrystals [As-prepared CZTS(e)]

The synthesis of CZTS(e) nanocrystals involved a controllable one-pot thermal decomposition method. For the synthesis of CZTS nanocrystals, 2 mmol $\text{Cu}(\text{OAc})_2 \cdot \text{H}_2\text{O}$, 1 mmol $\text{Zn}(\text{OAc})_2 \cdot 2\text{H}_2\text{O}$, 1 mmol $\text{SnCl}_2 \cdot 2\text{H}_2\text{O}$, and 4 mmol S were added into 40 mL OLA in a 100 mL three-neck flask on a Schlenk line. The mixture was degassed at 110 °C for 1 h, purged with N_2 for 30 min, and then heated to 280 °C for 1 h. The nanocrystals were purified and washed with cyclohexane and ethanol three times through centrifugation at 8000 rpm for 5 min. The black nanocrystals were collected and dried at 60 °C under vacuum overnight. The synthesis procedures of

the CZTSe nanocrystals were similar to those of CZTS, except that Se dissolution was used as anionic precursor, which was prepared by dissolving 4 mmol Se powder in oleylamine with the help of 4 mL chloroform by ultrasound.

2.3. Hydrophilic treatment of CZTS(e) nanocrystals [Hydrophilic CZTS(e)]

The as-prepared hydrophobic nanocrystals were rendered water soluble by following procedures: ~200 mg nanocrystals dispersed in 10 mL cyclohexane was mixed with 10 mL DMF solution containing ~100 mg $\text{Na}_2\text{S} \cdot 9\text{H}_2\text{O}$. The bi-phase system was vigorously shaken for 10 min to promote the phase transfer, resulting in the black nanocrystals move into the DMF phase, as shown in Fig. S1. Excluded the upper clear cyclohexane layer, the DMF phase was purified and washed three times with ethanol and water by centrifugation at 8000 rpm for 5 min. The S^{2-} modified hydrophilic nanocrystals were collected and dried at 60 °C under vacuum overnight.

2.4. Synthesis of ZnO microspheres and NYF microplates

The ZnO microspheres were synthesized by alcoholysis of zinc acetate [47]. Briefly, 30 mmol $\text{Zn}(\text{OAc})_2 \cdot 2\text{H}_2\text{O}$ was added into 300 mL diethylene glycol with stirring at 130 °C until completely dissolved, then further heated to 180 °C for 15 min. The white precipitate was collected and washed with ethanol and water, followed by drying at 200 °C in air.

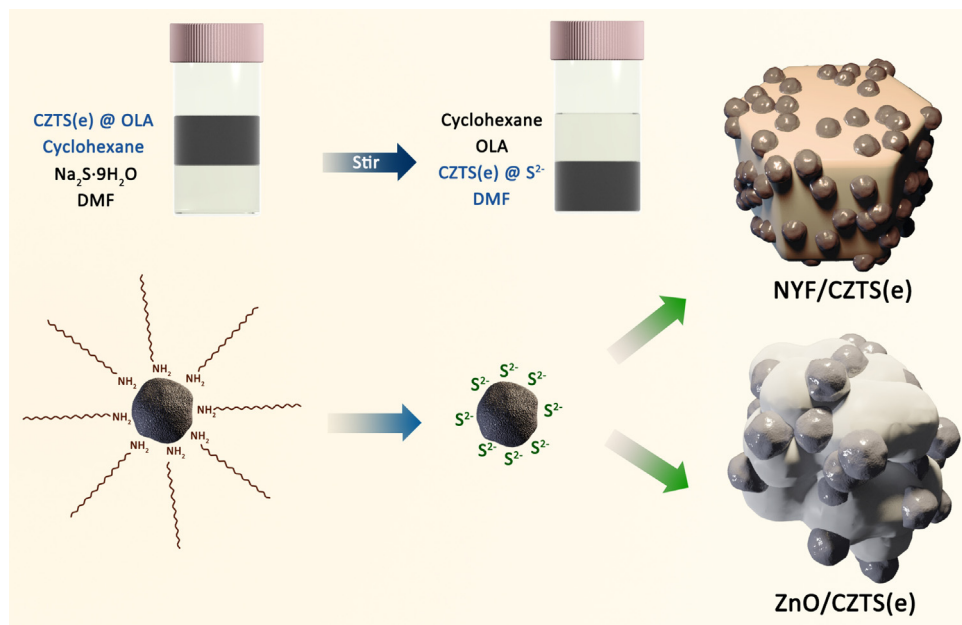
The NYF microplates were synthesized by a hydrothermal route [48]. 1.0 mmol $\text{YCl}_3 \cdot 6\text{H}_2\text{O}$, $\text{YbCl}_3 \cdot 6\text{H}_2\text{O}$, and $\text{TmCl}_3 \cdot 6\text{H}_2\text{O}$ (Y: Yb: Tm = 79.5: 20: 0.5 in molar ratio) aqueous solution was mixed with 0.75 mmol trisodium citrate aqueous solution, resulting a white complex. Then 12 mmol NaF aqueous solution was dropwise added into the complex under stirring (25 mL in total), followed by stirring for 1 h. The mixture was then transferred into a 40 mL autoclave and heated at 180 °C for 3 h. The products were washed three times with ethanol and water and collected via centrifugation, followed by annealing at 400 °C for 1.5 h in N_2 atmosphere.

2.5. Fabrication of CZTS(e) sensitized photocatalysts [$\text{ZnO}/\text{CZTS}(e)$ and $\text{NYF}/\text{CZTS}(e)$ hybrids]

The as-synthesized hydrophilic CZTS(e) nanocrystals and ZnO microspheres (NYF microplates) were taken separately (1:10 in molar ratio) in two containers and dispersed well in ethanol. Then the CZTS(e) dispersion was added dropwise into the ZnO (NYF) dispersion, and stirred overnight. After the solvent was evaporated out, the products were grinded and heat treated at 300 °C for 15 min in N_2 atmosphere.

2.6. Characterizations

Crystalline properties of the samples were analyzed by a powder X-ray diffractometer (XRD, SmartLab, Rigaku, Japan) using $\text{Cu K}\alpha$ radiation (40 kV, 30 mA), and a Raman spectrometer (Inviareflex, Renishaw, UK) equipped with a 514 nm laser. The morphologies of the samples were observed by a field emission scanning electron microscopy (SEM, Quatan 250FEG, FEI, USA), and a transmission electron microscopy (TEM, JEM-2100, JEOL, Japan). The surface modification of the samples were characterized by the Fourier transform infrared spectroscopy (FTIR, Nicolet 6700, Thermo Scientific, USA), and thermogravimetric analysis (TGA, STA449C, Netzsch, Germany) at a heating rate of 10 °C/min under N_2 atmosphere. Composition identification of the samples was performed by X-ray photoelectron spectroscopy (XPS, AXIS UltraBld, Kratos, UK) using monochromatic $\text{Al K}\alpha$ radiation (150 W, 15 kV,



Scheme 1. Schematic illustration of the hydrophilic treatment process, and formation of S^{2-} modified hydrophilic nanocrystals sensitized hybrids.

1486.6 eV). All the binding energies of the samples were referenced to the C 1 s peak (284.8 eV). UV-vis-NIR absorption spectra of the samples were measured by a UV/Vis/NIR spectrometer (V-570, Jasco, Japan). The fluorescence spectra of the samples were detected on a fluorescence spectrometer (PL, F4600, Hitachi, Japan) equipped with a 980 nm laser. Electron spin resonance (ESR) spectra of radicals spin-trapped by 5,5-dimethyl-1-pyrroline *N*-oxide (DMPO, 97%, Sigma-Aldrich) were examined on a Bruker Elexsys E500 spectrometer with setting center field 3360 G and microwave frequency 9.43 GHz. A 150 W Xe lamp equipped with 400 nm filter and a 980 nm laser were used as Vis and NIR light sources, respectively.

2.7. Photocatalytic activity measurements

Both the Vis and NIR light-driven photocatalytic activities of the as-prepared hybrid photocatalysts were evaluated by photodegradation of the RhB aqueous solution (10 mg/L) at ambient temperature. A 150 W Xe lamp equipped with 400–780 nm band-pass filter (500 mW/cm²) and >760 nm pass filter (600 mW/cm²) were used as Vis and NIR light sources for ZnO/CZTS(e) and NYF/CZTS(e) hybrid photocatalysts, respectively. Typically, 15 mg of photocatalyst was added into 50 mL of RhB aqueous solution. The solution was continuously stirred in the dark for 12 h to ensure the adsorption-desorption equilibrium before irradiation. The concentration of the residual RhB was monitored at a sequence of time intervals by the UV-vis spectrum at 554 nm to calculate the degradation rate based on the Beer-Lambert Law.

3. Results and discussion

3.1. Structural and morphological characterization of the nanocrystals

Fig. 1a and b demonstrate the XRD patterns of the as-prepared and hydrophilic CZTS and CZTSe nanocrystals, respectively. It is seen that all diffraction peaks can be clearly ascribed to the tetragonal kesterite structure (JCPDS No. 26-0575 and 70-8930), and no any other impurities are detected. Moreover, Raman scattering analysis further verifies the formation of pure phase. As shown in Fig. S2, peaks in Raman spectra confirm the pure phases of the

as-prepared and hydrophilic CZTS(e), respectively [49]. Therefore, either XRD or Raman measurement reveals a secondary phase, indicating the pure CZTS(e) nanocrystals. Fig. 1c and d show the TEM images of as-prepared CZTS and CZTSe nanocrystals with the average sizes of 12 ± 2 nm and 19 ± 3 nm, respectively. The selected area electron diffraction patterns (SAED) as seen in the inset of Fig. 1c and d shows high crystallization of the nanocrystals. Fig. 1e and f exhibit the high-resolution TEM (HRTEM) images of the nanocrystals, indicating their primarily ordered single-crystalline structure and have the interplanar d-spacing of 0.31 and 0.33 nm indexed to the (112) planes of CZTS(e), respectively.

3.2. TGA and FTIR characterization of the hydrophilic treatment process

After the hydrophilic treatment, organic ligands are removed, which is further certified by TGA and FTIR spectroscopy. Fig. 2a shows the mass loss of the as-prepared and hydrophilic CZTS nanocrystals as a function of temperature. A ~13% mass decrease is measured for the as-prepared CZTS nanocrystals when heated to 500 °C. Two distinct mass loss stages at 300–400 °C and 400–500 °C are observed, which are ascribed to the OLA + S and OLA + S + Sn volatilization, respectively [44,50]. By contrast, hydrophilic nanocrystals exhibit a mass loss of less than 5%, associated to the volatilization of S and Sn. In a word, the higher mass loss for the as-prepared nanocrystals is due to the decomposition of the OLA molecules, which are not present at the surface of hydrophilic nanocrystals. Fig. 2b shows the FTIR spectra of the as-prepared and hydrophilic CZTS nanocrystals. The obvious characteristic C–H vibration modes at 2854 and 2922 cm⁻¹, and a weak one at 2959 cm⁻¹ are respectively attributed to C–H stretching at C–C and C=C bands of original OLA molecules attached on the surface of as-prepared nanocrystals [51]. While these features disappear from the hydrophilic one, demonstrating that the hydrophilic treatment strategy using Na₂S effectively removes organic ligands from the nanocrystals. Moreover, there is no apparent shape variation after hydrophilic treatment, as shown in inset of Fig. 2a. It is expected that the long-chain ligands removed can eliminate the influence of the insulating barrier and promote the charge transfer in and out of the nanocrystals [43,51].

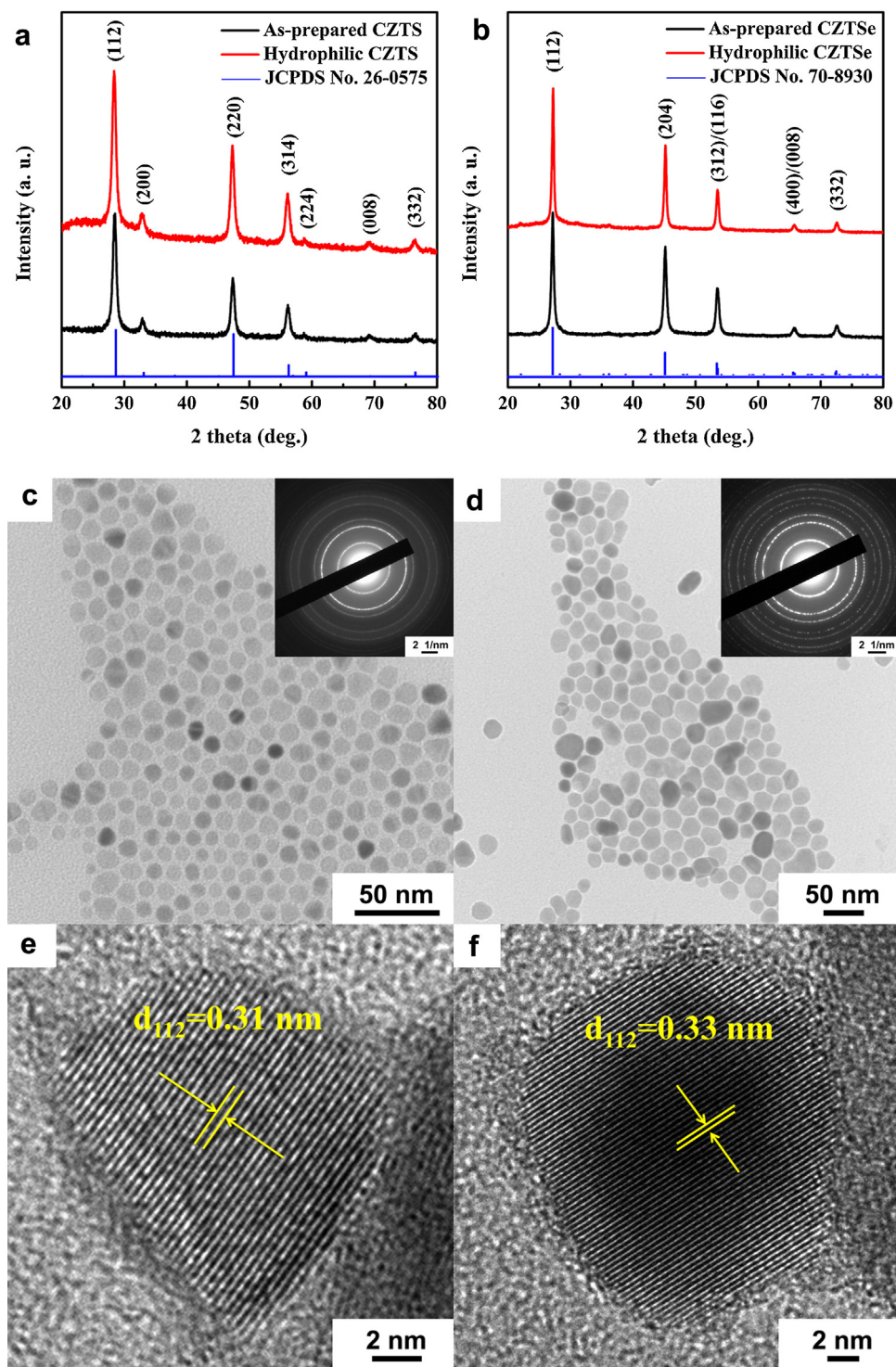


Fig. 1. XRD patterns of as-prepared (black line) and hydrophilic (red line) (a) CZTS and (b) CZTSe nanocrystals; TEM images of as-prepared (c) CZTS and (d) CZTSe nanocrystals (insets: the corresponding SAED patterns); and HRTEM images of as-prepared (e) CZTS and (f) CZTSe nanocrystals. (For interpretation of the references to colour in this figure legend, the reader is referred to the web version of this article.)

3.3. XPS analysis of the hydrophilic nanocrystals

XPS is used to investigate the chemical state of hydrophilic CZTS(e) nanocrystals. Fig. 3a reveals the Cu 2p core splitting into Cu 2p_{3/2} and Cu 2p_{1/2} peaks with a peak separation of 19.8 eV, and no satellite peak of Cu(II) at ~942 eV is observed, suggesting the Cu(I) oxidation state in the nanocrystals. Fig. 3b illustrates the Zn 2p peaks located at Zn 2p_{3/2} and Zn 2p_{1/2} with a peak separation

of 23.0 eV, consistent with Zn(II) oxidation state. Fig. 3c depicts an 8.4 eV separation of the Sn 3d_{5/2} and 3d_{3/2} peaks, indicating the Sn(IV) oxidation state. Fig. 3d exhibits the S 2p of CZTS core splits into S 2p_{3/2} and S 2p_{1/2} peaks with a peak separation of 1.1 eV, in good agreement with the expected S²⁻ in sulfide phase [52], and the Se 3d peak of CZTSe at 54.4 eV is representative of the binding energy for Se²⁻ [40].

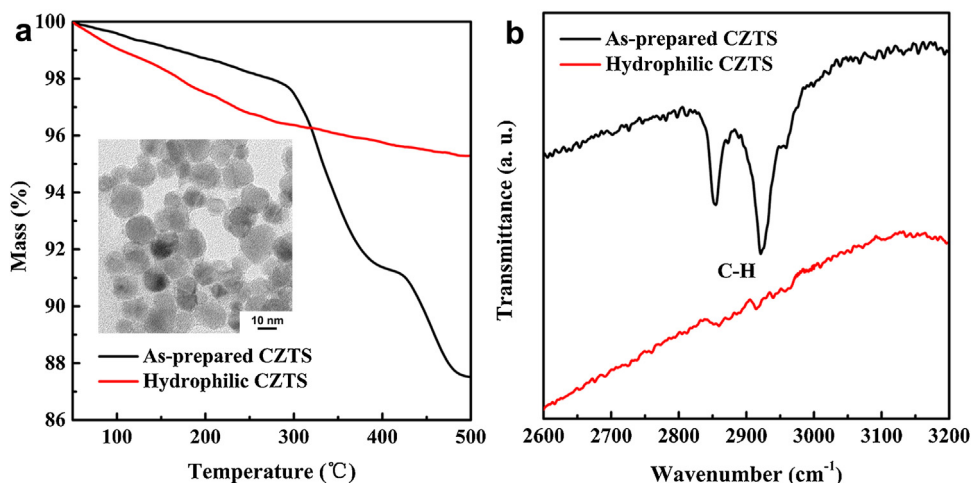


Fig. 2. (a) TGA and (b) FTIR spectra of as-prepared (blank line) and hydrophilic (red line) CZTS nanocrystals (inset of (a): TEM image of hydrophilic CZTS nanocrystals). (For interpretation of the references to colour in this figure legend, the reader is referred to the web version of this article.)

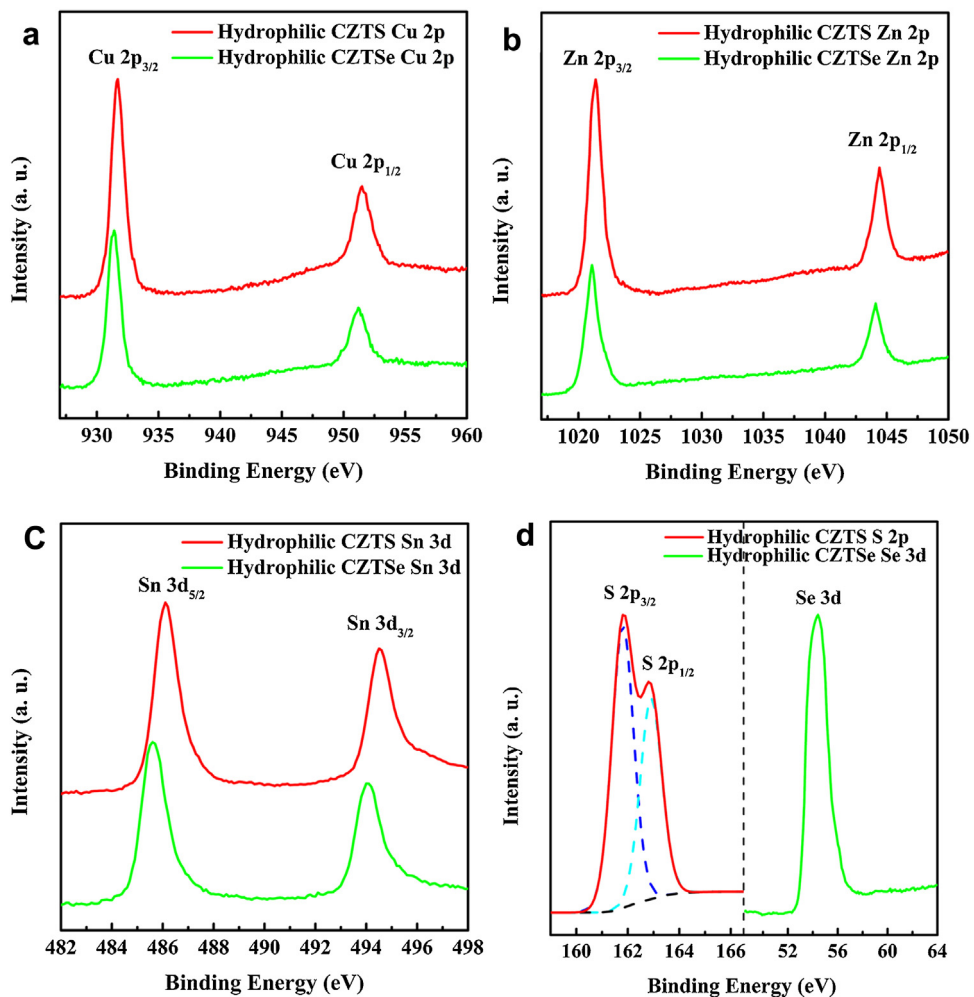


Fig. 3. XPS spectra of (a) Cu 2p, (b) Zn 2p, (c) Sn 3d, and (d) S 2p/Se 3d of hydrophilic CZTS (red line) and CZTSe (green line) nanocrystals. (For interpretation of the references to colour in this figure legend, the reader is referred to the web version of this article.)

3.4. Structural and morphological characterization of the hybrids

CZTS(e) nanocrystals alone have relatively low reactive activity in Vis light-driven photocatalytic reaction, and poor absorption of NIR light. As a proof of concept, the hydrophilic nanocrystals

are hybridized with ZnO and NYF as photosensitizers in Vis and NIR light-activated photocatalytic reactions, respectively. Fig. S3 exhibit the as-synthesized hexagonal phase ZnO microspheres with the average size of ~0.25 μm and hexagonal phase NYF microplates with the average size of ~1.65 μm. Two sets of diffraction peaks

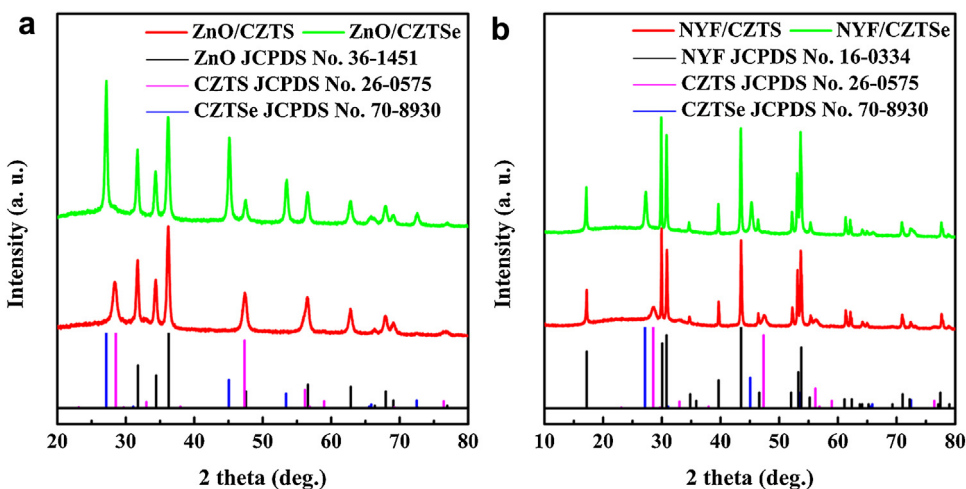


Fig. 4. XRD patterns of (a) ZnO/CZTS and ZnO/CZTSe, and (b) NYF/CZTS and NYF/CZTSe hybrids.

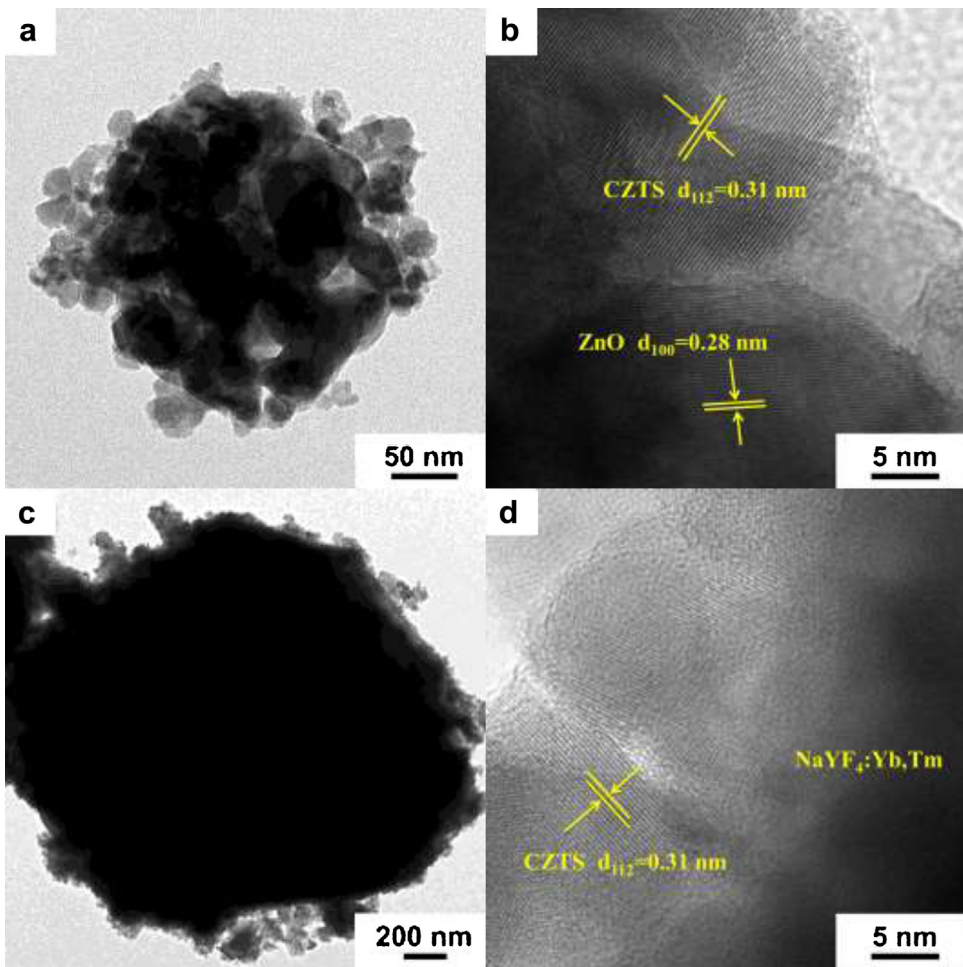


Fig. 5. TEM and corresponding HRTEM images of (a, b) ZnO/CZTS, and (c, d) NYF/CZTS hybrids.

appear in the XRD patterns of the ZnO/CZTS(e) and NYF/CZTS(e) hybrids, as shown in Fig. 4, which can be indexed to respective hexagonal phase ZnO (and NYF) (JCPDS No. 36-1451 and 16-0334) and tetragonal phases CZTS (and CZTSe) (JCPDS No. 26-0575 and 70-8930) clearly, respectively.

Fig. 5 show the representative TEM and HRTEM images of the ZnO/CZTS and NYF/CZTS hybrids. It can be observed from Fig. 5a

and c that the sphere-like or plate-like structures turn rough and uneven, indicating the coating of a secondary component. The black cores are the ZnO microspheres and NYF microplates, and the spots around the cores are CZTS nanocrystals. Under HRTEM, as shown in Fig. 5b and d, the clear lattice fringe 0.28 nm can be indexed to the distance of (100) plane of ZnO, and the lattice spacings of 0.31 are matched well with the (112) planes of the CZTS. The TEM and

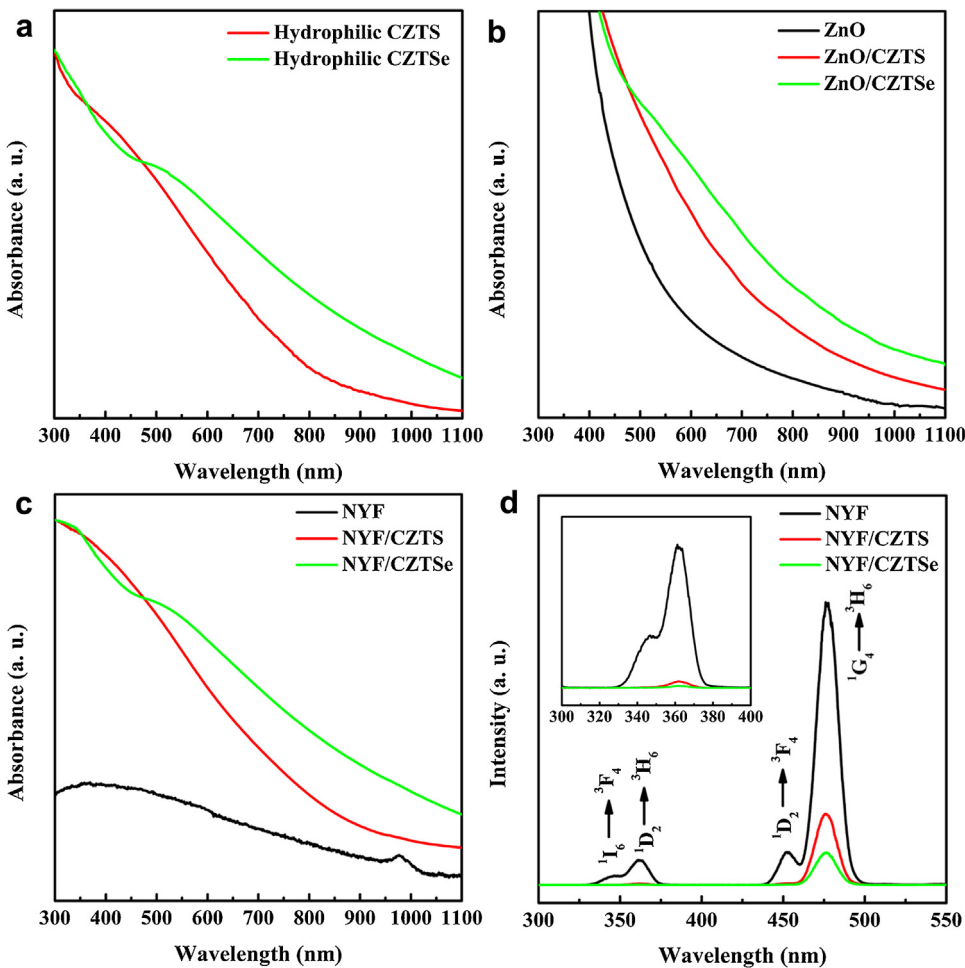


Fig. 6. UV-vis-NIR absorption spectra of (a) hydrophilic CZTS and CZTSe nanocrystals, (b) ZnO, ZnO/CZTS and ZnO/CZTSe hybrids, (c) NYF, NYF/CZTS and NYF/CZTSe hybrids; and (d) Upconversion PL spectra of NYF, NYF/CZTS and NYF/CZTSe hybrids (inset: enlarged PL spectra in 300–400 nm region).

HRTEM images of ZnO/CZTSe and NYF/CZTSe hybrids are exhibited in Fig. S4, which are similar to the ZnO/CZTS and NYF/CZTS hybrids, respectively.

3.5. Optical properties of the hydrophilic nanocrystals and hybrids

The optical absorption properties of the hydrophilic nanocrystals are represented in Fig. 6a. It can be seen that the absorption of the hydrophilic CZTS(e) nanocrystals cover the entire Vis and a little of NIR region. The bandgaps of the CZTS(e) are calculated from the following equation:

$$\alpha h\nu = A(h\nu - E_g)^{1/2} \quad (1)$$

where A , α , h , ν and E_g are a constant, the absorption coefficient, plank constant, light frequency and bandgap, respectively. The bandgaps of CZTS and CZTSe nanocrystals obtained from Fig. S5a are 1.53 and 1.32 eV, respectively. UV-vis-NIR absorption spectra of the ZnO microspheres and NYF microplates before and after sensitized by CZTS(e) nanocrystals are shown in Fig. 6b and c, respectively. The bandgap of ZnO is 2.99 eV, as shown in Fig. S5b. Before coating, the pure ZnO microspheres and NYF microplates do not have Vis light absorption. It is worth mentioning that the absorption peak around 980 nm of NYF microplates is contributed to the absorption of the Yb^{3+} ions [5]. When the nanocrystals are coated, strong Vis light absorptions are exhibited, suggesting the CZTS(e) nanocrystals act as sensitizers for trapping a large number of Vis photons. Fig. 6d displays the upconversion PL spec-

tra of the NYF microplates under the excitation of 980 nm laser. Four upcovered peaks are observed, including two UV emissions (346 nm and 362 nm) and two blue emissions (452 nm and 476 nm), which are assigned to the $^1\text{I}_6 \rightarrow ^3\text{F}_4$, $^1\text{D}_2 \rightarrow ^3\text{H}_6$, $^1\text{D}_2 \rightarrow ^3\text{F}_4$ and $^1\text{G}_4 \rightarrow ^3\text{H}_6$ transitions of Tm^{3+} ions, respectively [10]. Moreover, the absorption spectra of CZTS(e) nanocrystals can cover all four upconverted emissions of the NYF microplates. As shown in Fig. 6d and the enlarged inset, all four upcovered peaks intensity of hybrids dramatically decrease, which should be attributed to the absorption of the sensitizers. The significant enhanced ability of the ZnO/CZTS(e) and NYF/CZTS(e) to utilize Vis and NIR light makes them promising Vis and NIR light-activated photocatalytic reactions, respectively.

3.6. Photocatalytic performance of the hybrids

Photocatalytic activities of the ZnO/CZTS(e) and NYF/CZTS(e) hybrids are evaluated with degradation of RhB aqueous solution under Vis and NIR irradiation, respectively. Commercial available P25 TiO_2 (Degussa) is used for comparing. Obviously, no any RhB degradation is observed in the blank testing, indicating the stability of RhB solution under Vis and NIR irradiation. For the Vis light-driven photocatalytic reactions (Fig. 7a), only $\sim 35\%$, $\sim 40\%$, $\sim 30\%$ and $\sim 27\%$ of the RhB are photodegraded by using the P25, ZnO, CZTS and CZTSe alone after 120 min irradiation, while $\sim 92\%$ and $\sim 82\%$ are photodegraded by using the ZnO/CZTS and ZnO/CZTSe hybrids, showing significant enhanced photocatalytic activities. For the NIR light-driven photocatalytic reactions (Fig. 7b), there is almost no

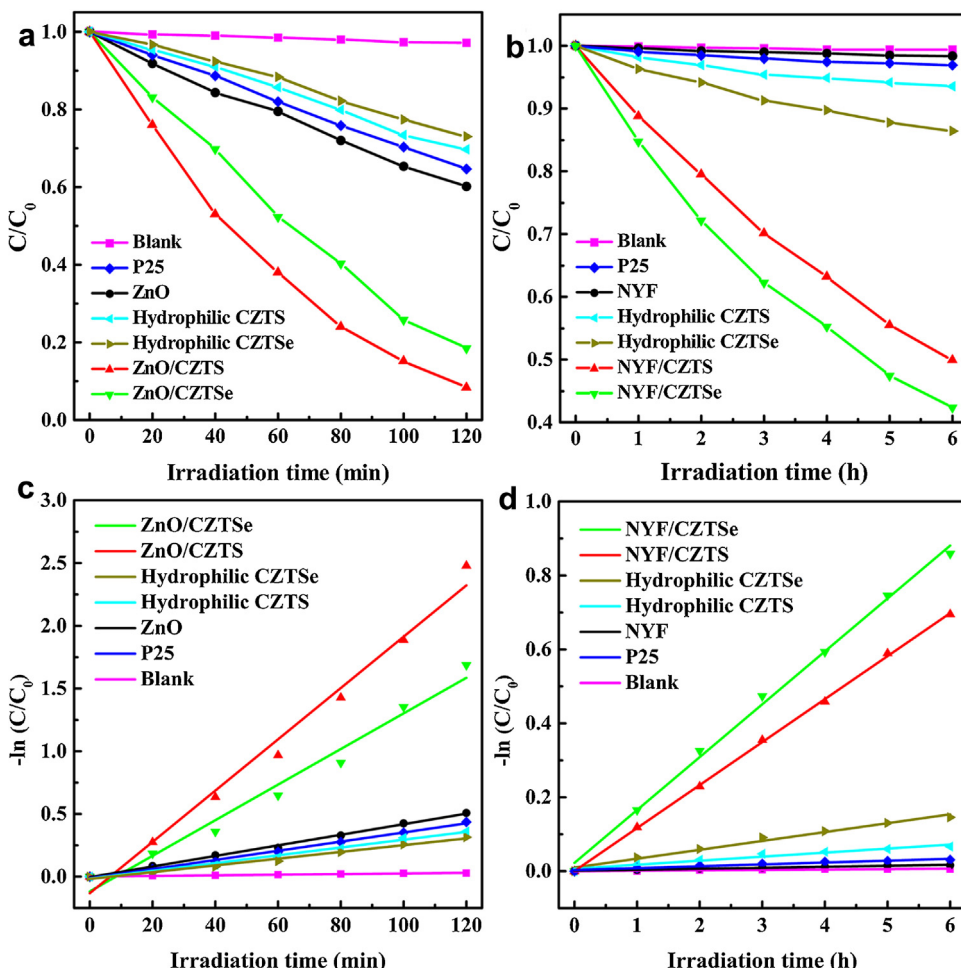


Fig. 7. (a) Vis and (b) NIR light-driven photocatalytic degradation of RhB; and (c, d) corresponding linear fitting results of pseudo-first-order kinetics.

Table 1
Calculated apparent rate constant k of RhB degradation for different photocatalysts.

Photocatalyst	$k \times 10^{-3} \text{ min}^{-1}$ (Vis)	$k \times 10^{-3} \text{ h}^{-1}$ (NIR)
P25	3.36	5.04
ZnO	4.22	/
NYF	/	2.70
CZTS	3.11	10.90
CZTSe	2.69	24.00
ZnO/CZTS	20.45	/
ZnO/CZTSe	14.20	/
NYF/CZTS	/	116.27
NYF/CZTSe	/	143.02

degradation for the P25 and pure NYF microplates, and a little photodegradation $\sim 7\%$ and $\sim 14\%$ are occurred for CZTS and CZTSe nanocrystals alone within 6 h. Remarkable enhanced photodegradation of $\sim 50\%$ and $\sim 58\%$ are obtained by inducing the NYF/CZTS and NYF/CZTSe hybrids. These results suggest that the hydrophilic CZTS(e) nanocrystals can serve as efficient photocatalytic sensitizers. A linear relation of photodegradation data can be easily fitted for all samples, as shown in Fig. 7c and d, indicating the pseudo-first-order kinetics photocatalytic process as follow:

$$-\ln(C/C_0) = kt \quad (2)$$

where C , C_0 and k are RhB concentration at time t and start, and apparent rate constant of RhB degradation, respectively. The calculated k values for all samples are summarized in Table 1. For the Vis light-driven photocatalytic reactions (Fig. 7c), the

k values of the P25, ZnO, CZTS and CZTSe are only 3.36 , 4.22 , 3.11 and $2.69 \times 10^{-3} \text{ min}^{-1}$, respectively. After deposition of the CZTS and CZTSe sensitizers, the k values increase to 20.45 and $14.20 \times 10^{-3} \text{ min}^{-1}$, which are almost 4.85 and 3.36 times higher than that of pure ZnO microspheres, respectively. For the NIR light-driven photocatalytic reactions (Fig. 7d), the small k values of 10.90 and $24.00 \times 10^{-3} \text{ h}^{-1}$ for CZTS and CZTSe dramatically increase to 116.27 and $143.02 \times 10^{-3} \text{ h}^{-1}$ after hybridized with NYF microplates, respectively.

3.7. Possible mechanisms of the enhanced photocatalytic performance

Above results indicate that the CZTS(e) nanocrystals can act as efficient photocatalytic sensitizers. To investigate the active radicals generated during the photocatalytic degradation process, DMPO spin-trapping ESR technique was employed to detect the superoxide radical ($\text{O}_2^{\bullet-}$) and hydroxyl radical (OH^{\bullet}). As shown in Fig. 8a, under light illumination, strong DMPO- $\text{O}_2^{\bullet-}$ signals can be clearly observed in both ZnO/CZTS and NYF/CZTS hybrids, indicating the massive production of $\text{O}_2^{\bullet-}$ in photocatalytic reactions. In Fig. 8b, four relatively weak characteristic peaks of DMPO- OH^{\bullet} in ZnO/CZTS hybrids are detected, suggesting the generation of OH^{\bullet} . While almost no such signal can be seen in NYF/CZTS hybrids due to the valence band (VB) of the CZTS is less positive than the standard potential of $\text{OH}^{\bullet}/\text{OH}^{\bullet-}$ and $\text{H}_2\text{O}/\text{OH}^{\bullet}$ [53]. Herein, we propose possible mechanisms for the enhanced photocatalytic activities of the hybrids. For ZnO/CZTS(e) hybrids, as illustrated in Scheme 2a,

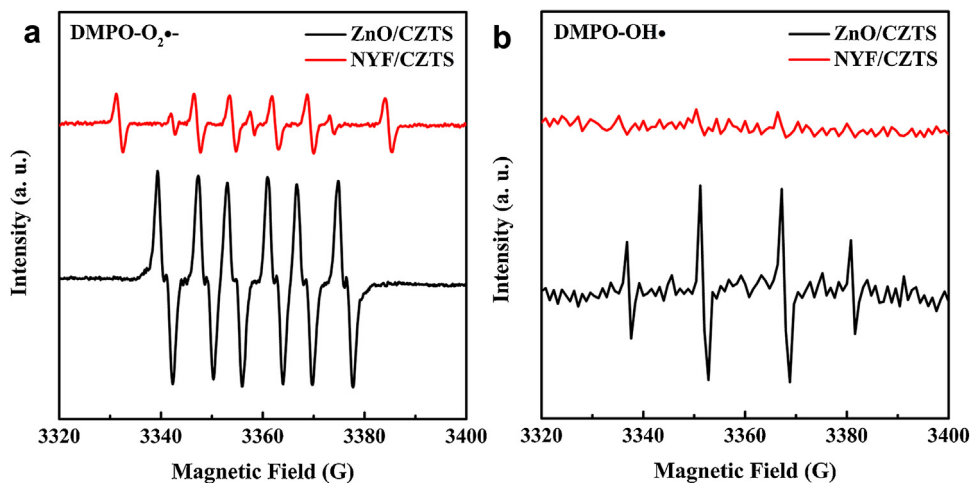
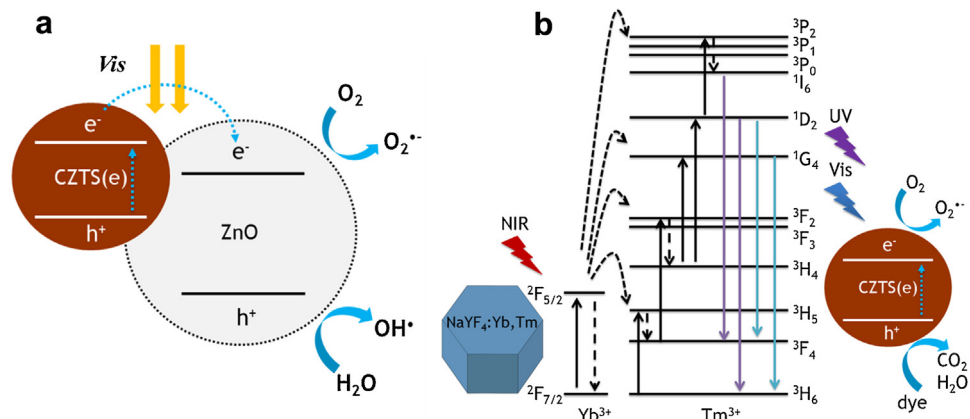


Fig. 8. DMPO spin-trapping ESR spectra of ZnO/CZTS (black line) and NYF/CZTS (red line) hybrids in (a) methanol dispersion for DMPO- $O_2^{\bullet-}$ and (b) aqueous dispersion for DMPO- OH^{\bullet} . (For interpretation of the references to colour in this figure legend, the reader is referred to the web version of this article.)



Scheme 2. Schematic illustration of (a) the energy band structure and the Vis light-driven photocatalytic degradation process of the ZnO/CZTS(e) hybrids, and (b) the energy levels for upconversion process and the NIR light-driven photocatalytic process of the NYF/CZTS(e) hybrids.

electrons are excited from VB to conduction band (CB) under illumination. The sensitizers improve the absorption efficiency through the entire Vis region, generating more electron-hole pairs. Moreover, the hybrid promotes the photogenerated electrons rapidly transfer from CZTS(e) to ZnO due to the lower CB of ZnO than that of CZTS(e) [54], and reduces the recombination of the electron-hole pairs. The photogenerated electrons are captured by O_2 in the aqueous solution to form $O_2^{\bullet-}$, which can degraded RhB into inorganic products. Simultaneously, the highly oxidative OH^{\bullet} generated from the holes can oxidize organic species into mineralized products. Thus, the enhanced photocatalytic activities are achieved due to the full utilization of the Vis light of the sensitizers, and high interfacial charge separation and transfer ability of the hybrids. Scheme 2b illustrates the possible photocatalytic mechanism of NYF/CZTS(e) hybrids under NIR irradiation. The NYF microplates serve as light transducers, and CZTS(e) nanocrystals are the catalytic part for generating reactive species. Firstly, the Yb^{3+} ions absorb the NIR light and relax from $^2F_{5/2}$ to the $^2F_{7/2}$ energy level, then successively transfer energy to the nearby Tm^{3+} ions. Secondly, the Tm^{3+} ions are excited successively to 1G_4 , 1D_2 and 1I_6 energy levels [10]. Thirdly, the excited Tm^{3+} ions fall to lower energy levels: $^1I_6 \rightarrow ^3F_4$, $^1D_2 \rightarrow ^3H_6$, $^1D_2 \rightarrow ^3F_4$ and $^1G_4 \rightarrow ^3H_6$, leading to UV and Vis light emission peak at 346 nm, 362 nm, 452 nm and 476 nm, respectively. Under the excitation of these emissions, the photoinduced electrons generated from CZTS(e) nanocrystals react with O_2 to produce $O_2^{\bullet-}$, which are the same as that of ZnO/CZTS(e) hybrids, while

the holes directly function as oxidants rather than produce OH^{\bullet} . Therefore, the improved NIR light-driven photocatalytic activities are realized due to the combination of strong upconversion ability of NIR photons to UV and Vis ones of the NYF microplates with the intense utilization of upconverted emissions of the sensitizers.

4. Conclusions

A chloroform-assistant Se dissolution in oleylamine (TOP and alkylthiol free) as the green precursor has been used for the robust preparation of quaternary selenide nanocrystals. High-quality monodisperse CZTS(e) nanocrystals have been prepared successfully by a one-pot thermal decomposition route. The hydrophilic nanocrystals have been further obtained through a bi-phase hydrophilic treatment process, which can replace the hydrophobic OLA ligands with inorganic S^{2-} . Then the hydrophilic CZTS(e) nanocrystals have been hybridized with ZnO microspheres and NYF microplates as photosensitizers in Vis and NIR light-driven photocatalytic reactions, respectively. Results indicate that the enhanced photocatalytic activities of the as-prepared ZnO/CZTS(e) and NYF/CZTS(e) hybrids are mainly ascribed to the efficient utilization of the Vis light and emissions upconverted from NIR light of the nanocrystals, respectively. This study is expected to provide a facile, green and robust approach for the development of advanced photocatalytic sensitizers with colloidal nanocrystals from wet-chemistry synthesis.

Acknowledgments

This work was supported by the Research Fund for the Doctoral Program of Higher Education of China (Grant No. 20120201130004), the National Natural Science Foundation of China (Grant No. 51502239), and the 111 Project of China (B14040). Y. P. Du gratefully acknowledge the financial aid from the start-up funding from Xi'an Jiaotong University, the Fundamental Research Funds for the Central Universities (2015qngz12), the NSFC (Grant No. 21371140), and the China National Funds for Excellent Young Scientists (Grant No. 21522106). The SEM and TEM work were conducted at International Center for Dielectric Research, Xi'an Jiaotong University, Xi'an, P. R. China.

Appendix A. Supplementary data

Supplementary data associated with this article can be found, in the online version, at <http://dx.doi.org/10.1016/j.apcatb.2016.07.022>.

References

- [1] H. Li, Y. Zhou, W. Tu, J. Ye, Z. Zou, *Adv. Funct. Mater.* 25 (2015) 998–1013.
- [2] Y. Wang, Q. Wang, X. Zhan, F. Wang, M. Safdar, J. He, *Nanoscale* 5 (2013) 8326–8339.
- [3] Y. Yuan, L. Ruan, J. Barber, S. Joachim Loo, C. Xue, *Energy Environ. Sci.* 7 (2014) 3934–3951.
- [4] W. Yang, X. Li, D. Chi, H. Zhang, X. Liu, *Nanotechnology* 25 (2014) 482001.
- [5] Y. Tang, W. Di, X. Zhai, R. Yang, W. Qin, *ACS Catal.* 3 (2013) 405–412.
- [6] W. Wang, M. Ding, C. Lu, Y. Ni, Z. Xu, *Appl. Catal. B: Environ.* 144 (2014) 379–385.
- [7] W. Su, M. Zheng, L. Li, K. Wang, R. Qiao, Y. Zhong, Y. Hu, Z. Li, *J. Mater. Chem. A* 2 (2014) 13486.
- [8] D. Xu, Z. Lian, M. Fu, B. Yuan, J. Shi, H. Cui, *Appl. Catal. B: Environ.* 142–143 (2013) 377–386.
- [9] W. Wang, Y. Li, Z. Kang, F. Wang, J.C. Yu, *Appl. Catal. B: Environ.* 182 (2016) 184–192.
- [10] M. Tou, Y. Mei, S. Bai, Z. Luo, Y. Zhang, Z. Li, *Nanoscale* 8 (2015) 553–562.
- [11] C. Li, F. Wang, J. Zhu, J.C. Yu, *Appl. Catal. B: Environ.* 100 (2010) 433–439.
- [12] S.V. Kershaw, A.S. Susha, A.L. Rogach, *Chem. Soc. Rev.* 42 (2013) 3033–3087.
- [13] J. Kolny-Olesiak, H. Weller, *ACS Appl. Mater. Interfaces* 5 (2013) 12221–12237.
- [14] D. Aldakov, A. Lefrançois, P. Reiss, J. Mater. Chem. C 1 (2013) 3756–3776.
- [15] J. Han, Z. Liu, K. Guo, B. Wang, X. Zhang, T. Hong, *Appl. Catal. B: Environ.* 163 (2015) 179–188.
- [16] Y. Yang, W. Que, X. Zhang, Y. Xing, X. Yin, Y. Du, *J. Hazard. Mater.* 317 (2016) 430–439.
- [17] T. Hong, Z. Liu, W. Yan, B. Wang, X. Zhang, J. Liu, J. Wang, J. Han, *Chem. Commun.* 51 (2015) 13678–13681.
- [18] T. Hong, Z. Liu, J. Zhang, G. Li, J. Liu, X. Zhang, S. Lin, *ChemCatChem* 8 (2016) 1288–1292.
- [19] C. Persson, *J. Appl. Phys.* 107 (2010) 053710.
- [20] S. Ji, T. Shi, X. Qiu, J. Zhang, G. Xu, C. Chen, Z. Jiang, C. Ye, *Sci. Rep.* 3 (2013) 2733.
- [21] S. Chen, A. Walsh, X.G. Gong, S.H. Wei, *Adv. Mater.* 25 (2013) 1522–1539.
- [22] D.B. Mitzi, O. Gunawan, T.K. Todorov, K. Wang, S. Guha, *Sol. Energy Mater. Sol. Cells* 95 (2011) 1421–1436.
- [23] F. Fan, L. Wu, S. Yu, *Energy Environ. Sci.* 7 (2014) 190–208.
- [24] P. Kush, K. Deori, A. Kumar, S. Deka, *J. Mater. Chem. A* 3 (2015) 8098–8106.
- [25] X. Yu, A. Shavel, X. An, Z. Luo, M. Ibanez, A. Cabot, *J. Am. Chem. Soc.* 136 (2014) 9236–9239.
- [26] T. Arai, S. Tajima, S. Sato, K. Uemura, T. Morikawa, T. Kajino, *Chem. Commun.* 47 (2011) 12664–12666.
- [27] J. Xu, X. Yang, Q. Yang, T. Wong, C. Lee, *J. Phys. Chem. C* 116 (2012) 19718–19723.
- [28] X. Hou, Y. Li, J. Yan, C. Wang, *Mater. Res. Bull.* 60 (2014) 628–633.
- [29] K. Maeda, K. Tanaka, Y. Fukui, H. Uchiki, *Sol. Energy Mater. Sol. Cells* 95 (2011) 2855–2860.
- [30] G. Suresh Babu, Y.B. Kishore Kumar, P. Uday Bhaskar, S. Raja Vanjari, *Sol. Energy Mater. Sol. Cells* 94 (2010) 221–226.
- [31] E. Thimsen, S.C. Riha, S.V. Baryshev, A.B.F. Martinson, J.W. Elam, M.J. Pellin, *Chem. Mater.* 24 (2012) 3188–3196.
- [32] Z. Wang, G.P. Demopoulos, *ACS Appl. Mater. Interfaces* 7 (2015) 22888–22897.
- [33] A. Shavel, D. Cadavid, M. Ibanez, A. Carrete, A. Cabot, *J. Am. Chem. Soc.* 134 (2012) 1438–1441.
- [34] U. Ghorpade, M. Suryawanshi, S.W. Shin, K. Gurav, P. Patil, S. Pawar, C.W. Hong, J.H. Kim, S. Kolekar, *Chem. Commun.* 50 (2014) 11258–11273.
- [35] A.S.R. Chesman, J. van Embden, N.W. Duffy, N.A.S. Webster, J.J. Jasieniak, *Cryst. Growth Des.* 13 (2013) 1712–1720.
- [36] J. Wang, J. Hu, Y. Guo, L. Wan, *NPG Asia Mater.* 4 (2012) e2.
- [37] C. Jin, P. Ramasamy, J. Kim, *Dalton Trans.* 43 (2014) 9481–9485.
- [38] A. Shavel, J. Arbiol, A. Cabot, *J. Am. Chem. Soc.* 132 (2010) 4514–4515.
- [39] S.C. Riha, B.A. Parkinson, A.L. Prieto, *J. Am. Chem. Soc.* 133 (2011) 15272–15275.
- [40] Y. Liu, D. Yao, L. Shen, H. Zhang, X. Zhang, B. Yang, *J. Am. Chem. Soc.* 134 (2012) 7207–7210.
- [41] C. Bullen, J. van Embden, J. Jasieniak, J.E. Cosgriff, R.J. Mulder, E. Rizzardo, M. Gu, C.L. Raston, *Chem. Mater.* 22 (2010) 4135–4143.
- [42] F. Fan, Y. Wang, X. Liu, L. Wu, S. Yu, *Adv. Mater.* 24 (2012) 6158–6163.
- [43] J. van Embden, A.S. Chesman, E. Della Gaspera, N.W. Duffy, S.E. Watkins, J.J. Jasieniak, *J. Am. Chem. Soc.* 136 (2014) 5237–5240.
- [44] A. Carrete, A. Shavel, X. Fontane, J. Montserrat, J. Fan, M. Ibanez, E. Saucedo, A. Pérez-Rodríguez, A. Cabot, *J. Am. Chem. Soc.* 135 (2013) 15982–15985.
- [45] A. Nag, M.V. Kovalenko, J.S. Lee, W. Liu, B. Spokoyny, D.V. Talapin, *J. Am. Chem. Soc.* 133 (2011) 10612–10620.
- [46] M.A. Boles, D. Ling, T. Hyeon, D.V. Talapin, *Nat. Mater.* 15 (2016) 141–153.
- [47] F. Shen, W. Que, Y. He, Y. Yuan, X. Yin, G. Wang, *ACS Appl. Mater. Interfaces* 4 (2012) 4087–4092.
- [48] Y. Sun, Y. Chen, L. Tian, Y. Yu, X. Kong, J. Zhao, H. Zhang, *Nanotechnology* 18 (2007) 275609.
- [49] X. Fontane, L. Calvo-Barrio, V. Izquierdo-Roca, E. Saucedo, A. Pérez-Rodríguez, J.R. Morante, D.M. Berg, P.J. Dale, S. Siebentritt, *Appl. Phys. Lett.* 98 (2011) 181905.
- [50] J. Scragg, P. Dale, D. Colombara, L. Peter, *ChemPhysChem* 13 (2012) 3035–3046.
- [51] C. Dun, W. Huang, H. Huang, J. Xu, N. Zhou, Y. Zheng, H. Tsai, W. Nie, D.R. Onken, Y. Li, D.L. Carroll, *J. Phys. Chem. C* 118 (2014) 30302–30308.
- [52] S.C. Riha, B.A. Parkinson, A.L. Prieto, *J. Am. Chem. Soc.* 131 (2009) 12054–12055.
- [53] Z. Zhou, P. Zhang, Y. Lin, E. Ashalley, H. Ji, J. Wu, H. Li, Z. Wang, *Nanoscale Res. Lett.* 9 (2014) 477.
- [54] Z. Dong, Y. Li, B. Yao, Z. Ding, G. Yang, R. Deng, X. Fang, Z. Wei, L. Liu, *J. Phys. D: Appl. Phys.* 47 (2014) 075304.